Journal of Biomedical Optics

BiomedicalOptics.SPIEDigitalLibrary.org

Investigation of reflectance sampling depth in biological tissues for various common illumination/collection configurations

George Zonios

SPIE.

Investigation of reflectance sampling depth in biological tissues for various common illumination/collection configurations

George Zonios*
University of Ioannina, Department of Materials Science and Engineering, 45110 Ioannina, Greece

Abstract. Knowledge of light penetration characteristics is very important in almost all studies in biomedical optics. In this work, the reflectance sampling depth in biological tissues was investigated using Monte Carlo simulations for various common illumination/collection configurations. The analysis shows that the average sampling depth can be described by two simple empirical analytical expressions over the entire typical ranges of absorption and scattering properties relevant to *in vivo* biological tissue, regardless of the specific illumination/collection configuration details. These results are promising and helpful for the quick, efficient, and accurate design of reflectance studies for various biological tissue applications. [DOI: 10.1117/1.JBO.19.9.097001]

Keywords: reflectance; scattering; Monte Carlo.

Paper 140353R received Jun. 4, 2014; revised manuscript received Aug. 12, 2014; accepted for publication Aug. 12, 2014; published online Sep. 8, 2014.

1 Introduction

Applications of optical reflectance spectroscopy for the noninvasive tissue analysis and investigation must often be tailored such that they provide information about specific tissue layers or structures. One reason for this is because pathologic conditions and tissue alterations are localized at specific tissue layers or morphological structures. For example, cancer arises in the epithelium, which typically occupies the top few hundred micrometers below the tissue surface. On the other hand, if one is interested in investigating tissue microcirculation, optical spectroscopy must be tuned such that it probes deeper tissue layers below the epithelium where microvessels are located. The main related parameter of interest is usually the sampling depth (or penetration depth) of light in tissue that determines the specific tissue layers being interrogated by optical spectroscopy.

In the simplest form of optical spectroscopy, visible light (often extended to include the near-infrared spectral region) enters the tissue at some point and the nonabsorbed part exits at some other point after having undergone multiple scattering. In this article, we investigate the sampling depth of reflectance spectroscopy using Monte Carlo simulations. Sampling depth in tissue depends on two main factors: illumination/collection geometry and tissue optical properties. By varying the illumination/collection geometry several different implementations of reflectance spectroscopy may be achieved with the main parameter affecting the final sampling depth of a particular implementation expected to be the separation (distance) between the point where light enters the tissue and the point where it exits and is detected.

Several popular illumination/collection geometry configurations used in biological tissue reflectance spectroscopy were investigated in this work, including single-optical fiber probes, six-around-one optical fiber probes, integrating sphere detectors, and diffuse reflectance configurations with illumination/collection separation larger than the transport scattering length in tissue. The goal of the investigation was to identify similar patterns and dependencies in the sampling depth characteristics of several different illumination/collection configurations and to provide a simple empirical (or semiempirical) formalism that can be used for the quick and efficient description of these sampling depth characteristics. These, in turn, could prove useful in the design of tissue reflectance studies and in choosing the appropriate reflectance geometry configuration suited for a particular application.

2 Methods

Monte Carlo simulations were used to calculate the penetration depth of light in tissue for various reflectance illumination/collection configurations. Tissue was assumed to be semi-infinite in extent (implemented as a 1000-cm-thick slab in the simulations) yielding zero transmission in all cases. For each different illumination/collection configuration, eight different values of the absorption coefficient (0.003, 0.01, 0.03, 0.1, 0.3, 1.0, 3.0, and 10.0 mm^{-1}) and four different values of the reduced scattering coefficient (0.5, 1.0, 1.5, and 3.0 mm^{-1}) were simulated yielding a total of 32 data points for each simulation geometry. The scattering anisotropy coefficient was assumed to be $g = 0.9$ and the tissue refractive index was 1.4. All the above tissue optical parameter values cover the typical ranges encountered for *in vivo* soft biological tissue.[1]

All simulations were implemented using the widely tested and used MCML code,[2] typically with 3 to 10 million photons per simulation. Some reflectance geometries (such as the 20-μm diameter single-fiber probe) required very long code execution times to yield satisfactory results. To overcome this limitation, a GPU parallel implementation of the MCML code was used (CUDAMCML),[3,4] which ran approximately 800 times faster than the original MCML CPU code and could simulate up to

*Address all correspondence to: George Zonios, E-mail: gzonios@cc.uoi.gr

0091-3286/2014/$25.00 © 2014 SPIE

a billion photons. The hardware used was an Intel i7-920 CPU and an Nvidia GTS 250 GPU.

The average sampling depth, $\langle z \rangle$, was calculated using Eq. (1),

$$\langle z \rangle = \frac{\sum_i w_i z_i}{\sum_i w_i}, \tag{1}$$

where w_i is the weight of the i'th reflected (and scored as collected) photon and z_i the average photon depth in tissue with the sum taken over all photons scored as the reflectance for the particular simulated configuration. MCML and CUDAMCML codes do not normally calculate $\langle z \rangle$ as defined in Eq. (1), but they were appropriately modified to perform this task. Both codes were extensively tested side by side to ensure that they produced identical results for the various simulated illumination/collection configurations that are described in more detail below.

2.1 *Single-Optical Fiber Probe*

In this geometry, both illumination and collection are by means of the same single-optical fiber. Due to its simplicity and other related advantages, this configuration has been extensively used and tested in biomedical optics.[5–7] Six different fiber diameters were simulated (20, 50, 100, 200, 400, and 1000 μm) with a uniform illumination profile and a collection acceptance angle of 15 deg, which approximately corresponds to the acceptance angle of optical fibers commonly used in tissue reflectance studies.

2.2 *Six-Around-One Optical Fiber Probe*

Optical probes consisting of one central optical fiber and six concentric surrounding optical fibers are commonly used in reflectance studies of biological tissues.[8,9] Simulations were performed assuming delivery of light through the middle fiber and collection via the six surrounding fibers. Optical probes consisting of three different fiber diameters were simulated (100, 200, and 400 μm) with a uniform illumination profile and a collection acceptance angle of 15 deg.

2.3 *Thin Beam Illumination*

In this configuration, illumination was simulated by means of an infinitesimally thin incident beam, and reflectance was collected over a circular area centered at the illumination beam. Two different collection areas were simulated with 0.1 and 1.0-mm diameters. This geometry is perhaps farther away from realistic configurations (compared with the previous ones), but has some potential modeling merits due to its simplicity. In addition, it has been previously used as an effective modeling framework for diffuse reflectance.[10] To facilitate comparison with the optical fiber configurations, the collection acceptance angle was approximately assumed to be similar to that of commonly used optical fibers (15 deg).

2.4 *Integrating Sphere*

This configuration differs from the previous two in the sense that it does not simulate optical fibers but it is otherwise similar to that of the single fiber. Illumination and collection were implemented over a circular area with a given diameter. Illumination was assumed to be uniform over the given area and collection was over all possible reflectance exit angles. Two different integrating sphere diameters were simulated (10 and 20 mm).

2.5 *Diffuse Reflectance*

In this configuration, illumination was by means of an infinitesimally thin beam and collection was at a specific distance away from the incident beam with that distance being larger than the transport scattering length. This is in contrast to all the previous optical fiber configurations where typical illumination and collection configurations were smaller than the transport scattering length. This configuration also differs from the integrating sphere configuration in the sense that it does not include a mix of small and large illumination/collection separations. Two configurations were simulated where collection was over a 0.1-mm-wide ring-shaped area centered at 5 and 10 mm away from the illumination beam with collection at all possible exit angles.

2.6 *Total Reflectance*

Finally, a configuration was simulated where all reflectance (total reflectance) was scored regardless of exit position and exit angle, whereas illumination was by means of an infinitesimally thin incident beam.

3 Results

3.1 *Single-Fiber Probe*

The reflectance sampling depth data from the single-fiber simulations can be described very well by Eq. (2),

$$\langle z \rangle = A e^{-b\sqrt{\mu_a}}, \tag{2}$$

where μ_a is the absorption coefficient and A, b are parameters which depend on the reduced scattering coefficient and fiber diameter. More specifically, Eq. (2) becomes Eq. (3) if the dependence on the reduced scattering coefficient is introduced

$$\langle z \rangle = a_1 (\mu_s')^{-b_1} e^{-a_2 (\mu_s')^{-b_2} \sqrt{\mu_a}} \tag{3}$$

with a_1, a_2, b_1, b_2 depending now only on the fiber diameter d. If the dependence on the fiber diameter is explicitly introduced in Eq. (3) then we arrive at Eq. (4), which is a full description of the reflectance sampling depth for single-fiber probes,

$$\langle z \rangle = c_1 d^{c_2} (\mu_s')^{-(e_1 + e_2\sqrt{d})} e^{-(f_1 + f_2\sqrt{d})(\mu_s')^{-0.178}\sqrt{\mu_a}}, \tag{4}$$

where d is the fiber diameter (in μm), μ_s' is the reduced scattering coefficient and $c_1 = 0.00594$, $c_2 = 0.612$, $e_1 = 0.280$, $e_2 = 0.0053$, $f_1 = 0.216$, and $f_2 = 0.0263$, with μ_a, μ_s' in mm^{-1}. Figure 1 shows the very good description of the simulation data provided by Eq. (4) for two representative values of the fiber diameter.

In addition to Eq. (2), it was found that the simulation results could also be described well by Eqs. (5) and (6)

$$\langle z \rangle = \frac{1}{a + b\sqrt{\mu_a}}, \tag{5}$$

$$\langle z \rangle = \frac{1}{a + b\mu_a}. \tag{6}$$

In both Eqs. (5) and (6), a and b are parameters (different for each equation) that depend on the reduced scattering coefficient

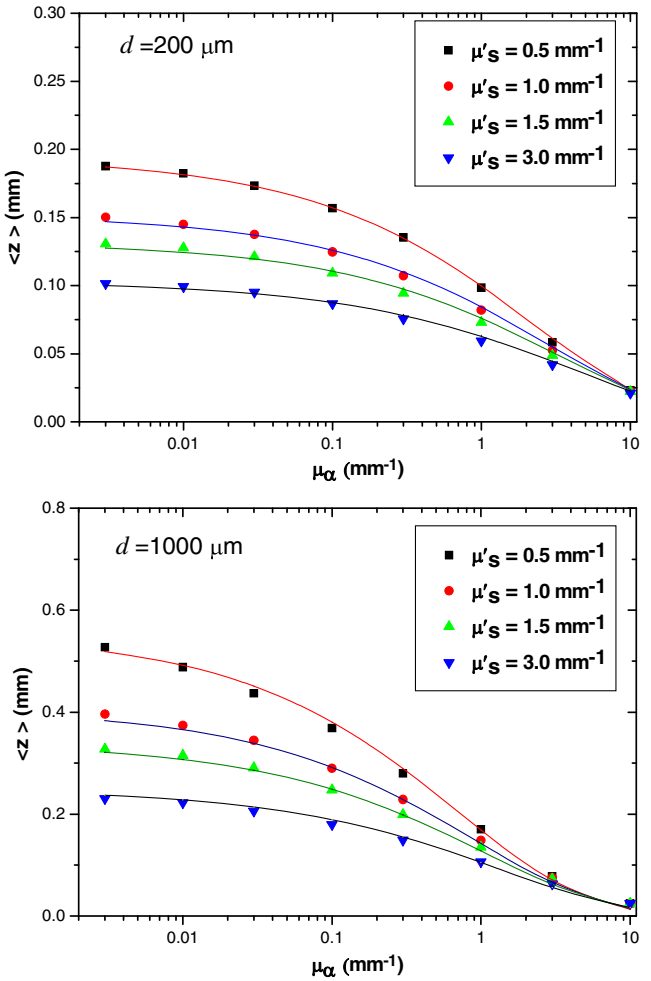

Fig. 1 Fits to Eq. (4) (solid lines) for the single-fiber probe simulation data, for two different fiber diameters.

and fiber diameter. Figure 2 shows the performance of Eqs. (2), (5), and (6) in describing the simulation data by showing the r^2 coefficient of the corresponding fits. Equation (2) provides an excellent description of the data, but Eqs. (5) and (6) also describe the data very well and can potentially be used as the basis for the development of more general expressions for the

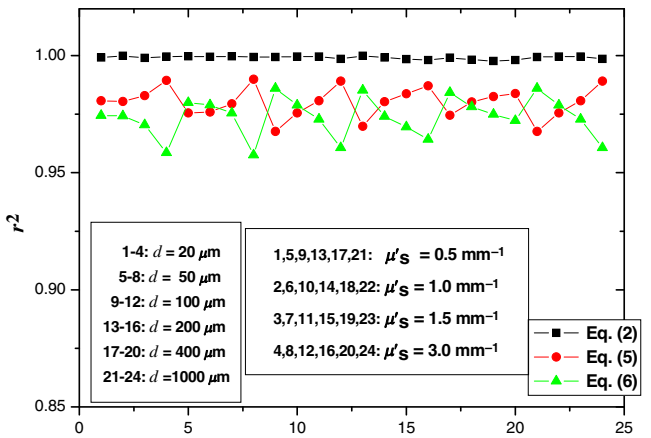

Fig. 2 Goodness of fit coefficient (r^2) for the single-fiber probe data, fitting to Eqs. (2), (5), and (6). Equation (2) offers an excellent description of the data regardless of fiber diameter.

reflectance in a manner similar to that of Eqs. (3) and (4), especially when great accuracy is not needed.

3.2 *Six-around-One Probe*

Equations (2), (5), and (6) were found to describe the simulation results well as shown in Fig. 3, with Eqs. (2) and (5) performing better than Eq. (6). As in the case of the single-fiber probe, Eq. (2) was chosen as the basis for the construction of a compact analytical expression describing sampling depth for a six-around-one probe made out of 200-μm diameter optical fibers. The resulting analytical expression is described by Eq. (3), with $a_1 = 0.349$, $a_2 = 0.696$, $b_1 = 0.426$, and $b_2 = 0.214$, where these last four parameters can potentially be expressed as a function of fiber diameter in a manner similar to that of Eq. (4) for the single-fiber probe, in case one wants to construct a more general expression than that of Eq. (3). Figure 4 illustrates how well Eq. (3) describes the simulation results for the probe consisting of 200-μm diameter optical fibers.

Note that even though a different illumination/collection is examined here, a concise analytical expression describing the reflectance sampling depth can still be constructed using the

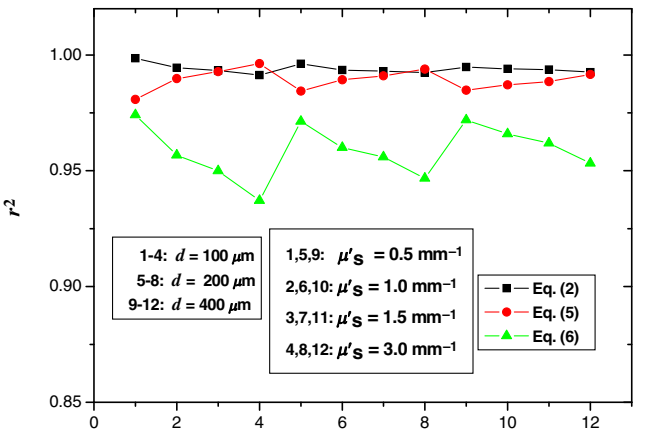

Fig. 3 Goodness of fit coefficient (r^2) for six-around-one optical fiber probe data, fitting to Eqs. (2), (5), and (6). Equation (2) offers the best description of the data, but Eq. (5) also gives good fits.

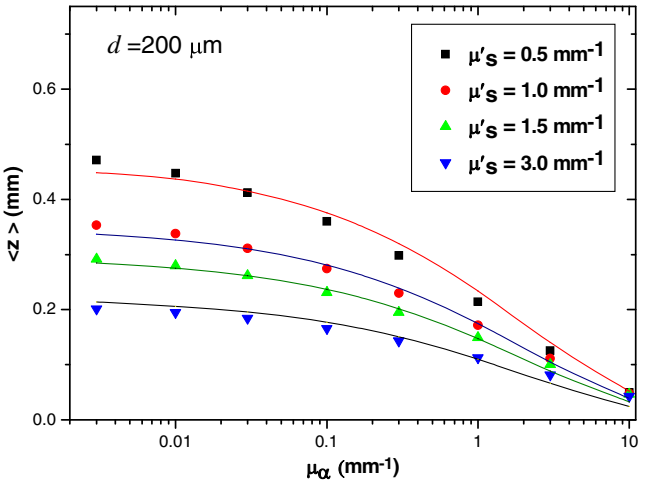

Fig. 4 Fits to Eq. (3) (solid lines) for the six-around-one optical fiber probe data, for a specific optical fiber diameter.

same Eq. (3). This points to the fact that as far as sampling depth is concerned, the exact details of the illumination/collection geometric configuration are not as important as the average (or effective) illumination collection separation. A consequence of this observation would be that Eqs. (2) and (3) could potentially be used for a wide range of illumination/collection configurations characterized by separations smaller than ~1 mm. This hypothesis is tested in Sec. 3.3, which examines illumination via an infinitesimally small thin beam and collection in a circular area centered at the illumination beam.

3.3 *Thin Beam Illumination*

Figure 5 shows that Eq. (2) performs better than Eqs. (5) and (6) in describing the thin beam illumination simulation results. Using it as the basis for the development of a concise analytical expression for the description of the 100-μm diameter collection area sampling depth (as in the two previous cases of single fiber and six-around-one probe), we arrive again at Eq. (3) with $a_1 = 0.0941$, $a_2 = 0.451$, $b_1 = 0.3476$, and $b_2 = 0.1478$. Figure 6 shows the performance of Eq. (3) in describing the simulation results. As in the previous cases, the description is very good. The important observation here is that despite the three different illumination/collection configurations that have been presented so far, a single expression, Eq. (3), can be used to describe the sampling depth in all three cases.

3.4 *Integrating Sphere*

Figure 7 shows the performance of Eqs. (2), (5), and (6) in describing the simulation data. In contrast to the two previous configurations, here, it is Eq. (5) that appears to generally perform better even though Eq. (2) still outperforms Eq. (5) for small values of the reduced scattering coefficient and the small diameter of the integrating sphere. Thus, we choose Eq. (5) as the basis for the development of an analytical expression to describe the simulation data of the 20-mm diameter integrating sphere. The result is Eq. (7),

$$\langle z \rangle = \frac{1}{a_1(\mu_s')^{b_1} + a_2(\mu_s')^{b_2}\sqrt{\mu_a}}, \tag{7}$$

where $a_1 = 0.5752$, $a_2 = 3.797$, $b_1 = 0.6352$, and $b_2 = 0.6069$. Figure 8 shows the performance of Eq. (7) in describing

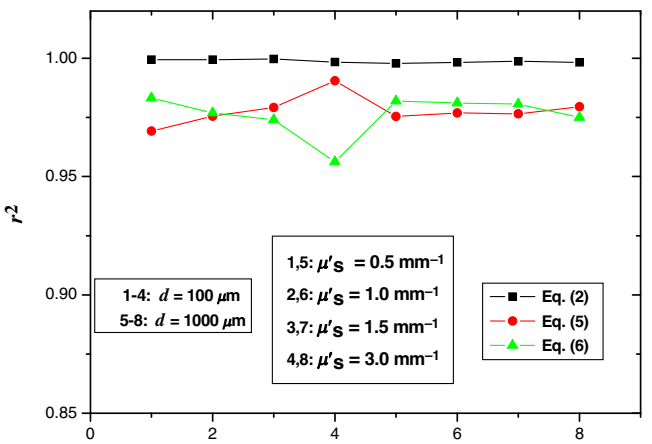

Fig. 5 Goodness of fit coefficient (r^2) for the thin beam illumination data, fitting to Eqs. (2), (5), and (6). Equation (2) offers the best description of the data.

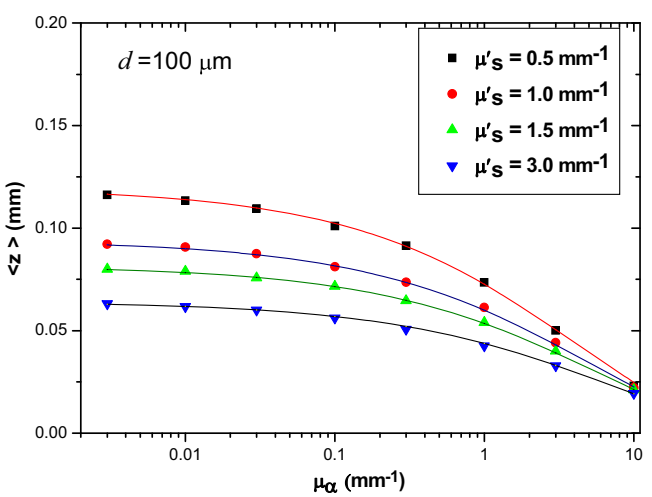

Fig. 6 Fits to the thin beam illumination data for a given collection circle diameter. Solid lines represent the fits to Eq. (3).

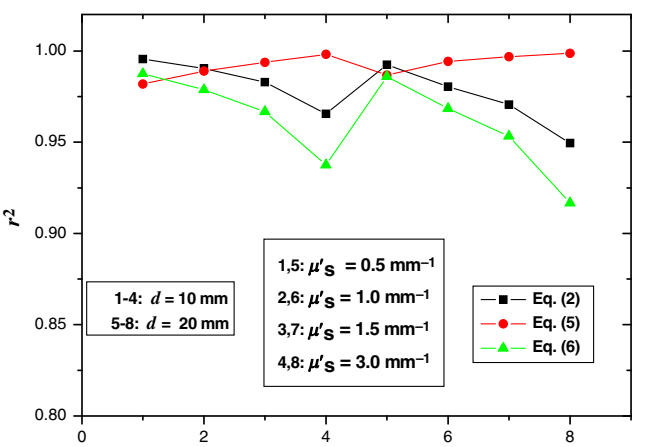

Fig. 7 Goodness of fit coefficient (r^2) for the integrating sphere data, fitting to Eqs. (2), (5), and (6). Equation (5) offers the best description of the data, while Eq. (2) also performs well.

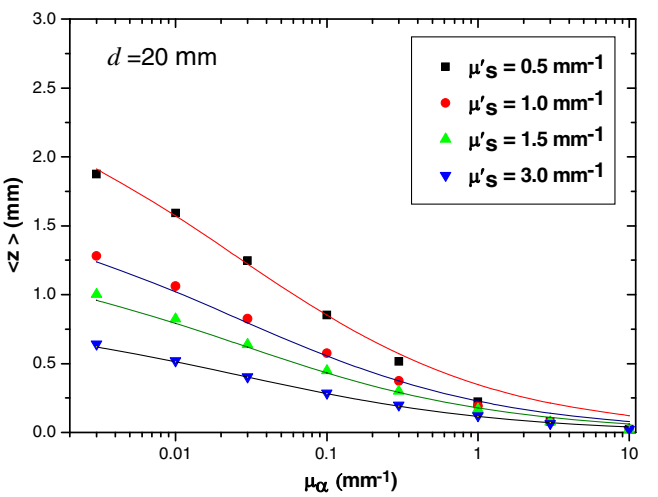

Fig. 8 Fits to the integrating sphere data for a given sphere diameter. Solid lines represent the fits to Eq. (7).

the simulation data. The main observation here is that as we move to larger illumination/collection separations, Eq. (5) becomes more suitable for the description of sampling depth than Eq. (2). Note, though, that the integrating sphere geometry includes a mix of small and large illumination/collection separations and thus Eq. (2) still performs well. The other interesting observation here is that the dependence on the reduced scattering coefficient has the same functional form (power law) in both Eqs. (3) and (7).

3.5 *Diffuse Reflectance*

In this configuration, the illumination/collection separation is larger than the transport scattering length, unlike all the previous configurations presented so far. Figure 9 shows the performance of Eqs. (2), (5), and (6) in describing the data for the 10-mm illumination collection separation. Equation (5) clearly has the advantage here in describing the data even though Eq. (2) still offers a reasonable performance that could be useful. Using Eq. (5) as the starting point, we arrive at Eq. (8) for the description of the sampling depth

$$\langle z \rangle = \frac{1}{a + b_1 e^{-b_2/\mu_s'} \sqrt{\mu_a}}, \tag{8}$$

where $a_1 = 0.2459$, $b_1 = 1.528$, and $b_2 = 0.260$. These three parameters can be potentially expressed as a function of illumination/collection separation to arrive at a more general expression for the diffuse reflectance configuration sampling depth. Figure 10 shows the performance of Eq. (8) in describing the sampling depth data for the 10-mm illumination/collection separation.

3.6 *Total Reflectance*

Figure 11 shows the performance of Eqs. (2), (5), and (6) in describing the total reflectance data. Note here the superior performance of Eq. (5) in describing the data while Eqs. (2) and (6) offer a rather poor description. Hence, Eq. (7) with $a_1 = 0.323$, $a_2 = 4.432$, $b_1 = 0.894$, and $b_2 = 0.559$ was found to describe the data very well, as is illustrated in Fig. 12. It is interesting to note that, as in the case of the integrating sphere configuration,

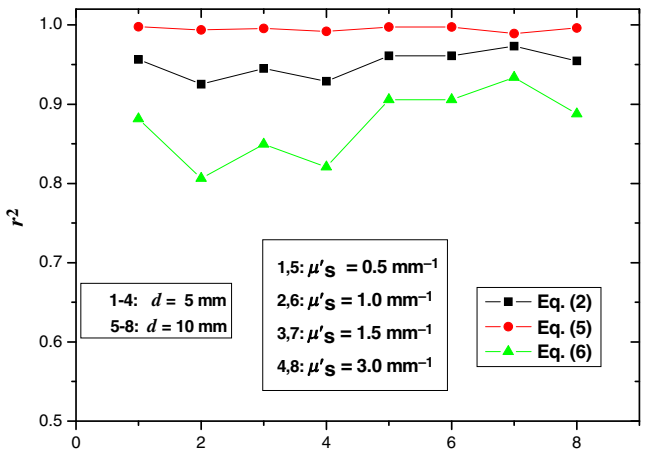

Fig. 9 Goodness of fit coefficient (r^2) for diffuse reflectance data, fitting to Eqs. (2), (5), and (6). Equation (5) offers the best description of the data.

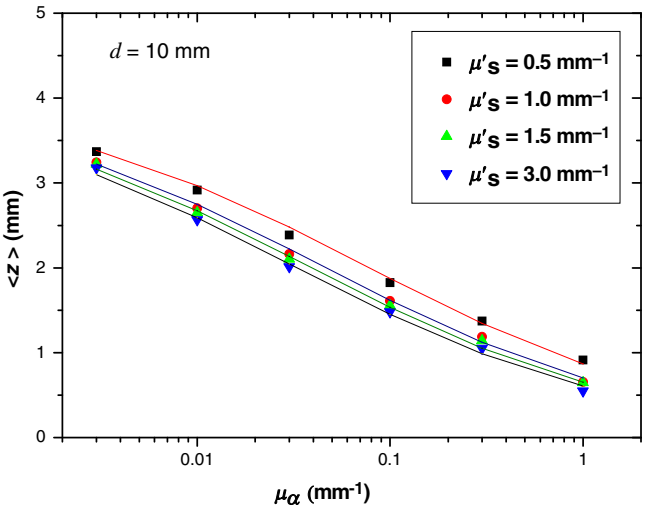

Fig. 10 Fits to the diffuse reflectance data for a specific illumination/collection configuration. Solid lines represent the fits to Eq. (8).

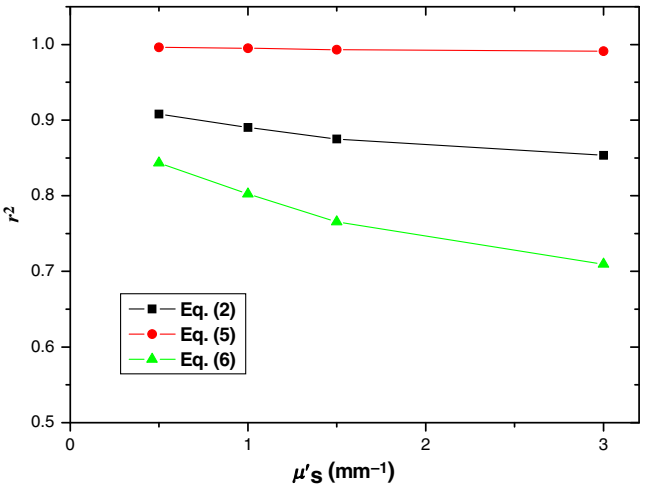

Fig. 11 Goodness of fit coefficient (r^2) for total reflectance data, fitting to Eqs. (2), (5), and (6). Equation (5) clearly offers the best description of the data.

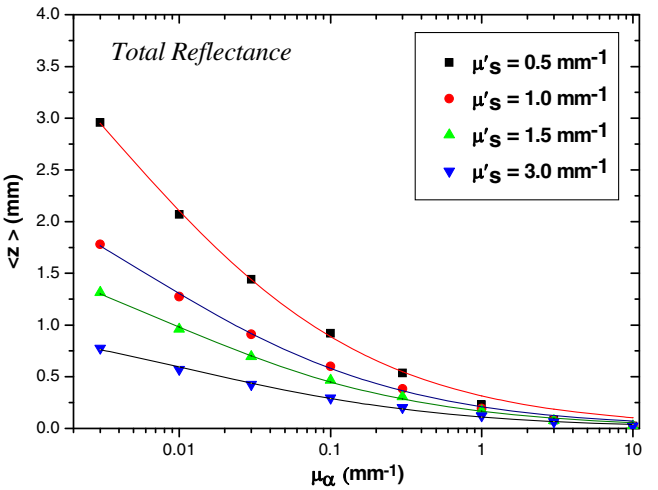

Fig. 12 Fits to the total reflectance data. Solid lines represent the fits to Eq. (7).

the total reflectance configuration includes a mix of both large and small illumination/collection separations and thus it is not surprising that Eq. (7) offers very good descriptions of the sampling depth data in both the integrating sphere and the total reflectance cases.

4 Discussion

The results of this simulation study indicate that the reflectance sampling depth in biological tissue can be described by two simple analytical expressions [Eqs. (2) and (5)], as a function of absorption, regardless of the specific illumination/collection configuration details. Moreover, these simple expressions can be used as the basis for the development of concise analytical expressions for more complete and specific description of sampling depth as a function of the absorption and reduced scattering coefficients as well as other geometric parameters of a particular illumination/collection geometrical configuration (e.g., fiber diameter or probe diameter). More specifically, Eq. (2) was found to provide a very good description of the sampling depth for most configurations and, in particular, it was found to provide an excellent description for illumination/collection separations approximately equal to or smaller than the transport scattering length. Equation (5) was also found to provide a very good description of the sampling depth but with a distinctly better performance for larger illumination/collection separations than the transport scattering length. Finally, Eq. (6), the simplest and most straightforward, even though it was generally found to perform worse than Eqs. (2) and (5), was also found to provide an adequate description of the sampling depth for most configurations studied, especially when some imperfections can be tolerated.

It is important to point out that the reflectance sampling depth is, because of its own nature, a quantity that cannot be defined or precisely measured. In practice, what is usually needed is an estimate of the sampling depth characteristics of a particular reflectance configuration and, in that light, imperfections in some model fits presented earlier in this study are not as critical as in the modeling of other physical quantities. In that spirit, we have tried to keep the analytical expressions developed to describe the sampling depth as simple as possible, perhaps sacrificing some small part of their accuracy in some cases. Also, in that spirit, we have included in our analysis the performance of Eq. (6) which, despite its general poorer performance, may still be of interest in some cases where simplicity may be preferred over accuracy. Also, Eq. (6) was included, again because of its simplicity, in order to serve as a simple baseline reference point. Finally, Eq. (6) has the additional advantage that it is not entirely empirical in nature, but it resembles the expression that one would get if a simple exponential attenuation due to absorption in tissue was considered.

One important observation from the present analysis is that the average illumination/collection separation distance appears to be the most important parameter affecting the sampling depth, with the particular details of a specific illumination/collection configuration coming second in terms of importance. Thus, Eq. (2), for example, was found to provide a nearly excellent description of the sampling depth of both single fiber and six-around-one fiber configurations as far as these are characterized by approximately the same average illumination/collection separation, which is smaller than the transport scattering length. This indicates that Eq. (2) has the potential to provide a very good description of the sampling depth of other illumination/collection reflectance configurations that are not covered in this study as long as these other configurations are characterized by similar illumination/collection separation features. Therefore, the modeling approach for the description of sampling depth presented in this work maybe of general value for many other different illumination/collection reflectance configurations. Similar comments can be made about Eq. (5) which was found to describe the sampling depth for configurations which include illumination/collection separations larger than the transport scattering length very well.

The influence of the illumination/collection separation can also be seen by observing the specific shape of the curves shown in Figs. 1, 4, 6, 8, 10, and 12. Thus, the curves shown in Figs. 1, 4, and 6 have approximately the same shape and general qualitative characteristics because they all correspond to small illumination/collection separations. On the other hand, the curve shapes appearing in Figs. 8, 10, and 12 differ (from those in Figs. 1, 4, and 6) because they include larger separations, with the difference being more prominent in Fig. 12 which includes all possible separations (with the larger ones perhaps dominating the picture).

In this work, a simple one-layer semi-infinite tissue model was employed. Although the utility of this model is well established in biomedical optics, it is still far from the realistic multilayered tissue picture. However, multilayered tissue structures can be implemented in MC simulations in a straightforward way and thus the modeling approach and methodology presented in this work could potentially be extended to cover the reflectance sampling depth of various multilayered biological tissues.

We have also not examined in full detail the effects of various scattering phase functions in modeling the sampling depth in tissue. This is because the Heney-Greenstein phase function with $g = 0.9$ is generally accepted as a reasonable description of average scattering anisotropy in soft biological tissues.[1,11,12] In addition, other studies have already investigated the effects of varying the scattering anisotropy in sampling depth and found it to have a rather minor effect for most common illumination/collection configurations.[5,12] Our limited exploration of the effects of anisotropy on sampling depth yielded results similar to those of previous studies. For example, we found that for the six-around-one probe with 200-μm diameter optical fibers, three different values of the scattering anisotropy ($g = 0.7$, 0.9, and 0.95) did not affect the sampling depth more than ~10%. Typically, increasing anisotropy resulted in a slight increase in sampling depth. Nevertheless, it must be pointed out that the modeling approach presented in this work could be extended to include additional parameters such as scattering anisotropy or various different scattering phase functions and this could be the subject of future investigations.

In the present work, we have adopted Eq. (1) for the description of the sampling depth. However, it should be noted that there are no unique and preferable descriptions of the sampling depth and other definitions have been employed in previous studies.[5,12] In Eq. (1), the average depth of photons is used whereas another popular definition uses the maximum depth of each photon.[12] We have investigated the relationship between the two definitions and found that, remarkably, the definition based on the maximum photon depth consistently yields a value of the sampling depth that is approximately twice that which is based on the average depth. We have found this statement to be valid for the entire range of absorption and scattering

coefficient values used in the present work and also for all various illumination/collection geometries studied. Hence, it appears that it would be rather straightforward going from one definition to the other; one can use either the average or maximum photon depth in Eq. (1), and scale the final results by an approximate factor of two. In more detailed analysis, we found that the ratio of the average sampling depth to the maximum sampling depth varies, in most cases, in the range 47% to 53% depending on the optical properties of tissue and the specific illumination/collection configuration simulated. Overall, this is an interesting finding that must be fully confirmed with a more detailed investigation.

In the present work, we have obviously not exhausted all possible illumination/collection reflectance geometries lest the whole endeavor would appear cumbersome and the resulting analysis would probably seem encyclopedic. Techniques such as differential path length reflectance[13] and polarized reflectance[12] have not been covered. It should be noted, though, that the modeling work presented here can be easily extended to cover these and other reflectance configurations. As already stated above, the important parameter affecting modeling appears to be (unsurprisingly) the illumination/collection separation hence there is no indication that the applicability of the present modeling approach could be limited to specific reflectance geometries.

We have also performed a limited investigation on the effects of detection acceptance angle in sampling depth. The results indicate that the sampling depth is not greatly affected by the collection acceptance angle even though the limited acceptance angle of fiber optic probes (compared to the full detection at all reflectance exit angles) yields a slight general increase in the sampling depth (10% to 20% typically, depending on the particular tissue optical properties and geometric configuration). This also confirms the fact that the illumination/collection separation seems to be the single most important parameter that drastically affects reflectance sampling depth.

In addition to the sampling depth itself, the sensitivity of the sampling depth on the tissue optical properties and other geometrical parameters is also important. Even though we have not directly addressed the sensitivity issue in this work, it should be pointed out that the sensitivity can be directly calculated from the expressions of sampling depth such as Eqs. (3), (4), (7), and (8). This is, of course, one of the important advantages that come with the development of simple analytical expressions for the sampling depth.

As already stated above, the sampling depth is a central and important quantity that needs to be considered and investigated in almost any reflectance study of biological tissue. Thus, it has been extensively studied both theoretically and experimentally. Gomes and Backman[12] have recently provided a review of many of the existing studies for various reflectance configurations. Compared to the existing literature, the important result of the present work is that it provides a simple picture with only two different empirical expressions as the basis, covering a wide range of reflectance configurations. Also, one other study[5] has reported a simple empirical expression providing a description of the sampling depth for single fiber probes. We have compared our Eq. (4) to the result of that study, and found that they are in good agreement (after the different definition of sampling depth is accounted for), with our Eq. (4) having the advantage of being simpler. In addition, Eq. (4) has the additional advantage that it is not based on (and does not require) knowledge of the "effective mean photon path length" in tissue as defined by Eq. (2) in Ref. 5.

Finally, a comment should be made on the great utility of the CUDA accelerated MCML code.[3,4] This code provides execution times that can be up to three orders of magnitude faster than those of the original MCML code, especially when one is interested in reflectance studies only and not in a detailed description of the internal distribution of light in biological tissue. Most importantly, this significant acceleration in execution time comes at essentially no additional cost with the graphics processing units available today.

5 Conclusions

- Sampling depth can be described (as a function of absorption) by two simple empirical analytical expressions for a wide range of illumination/collection configurations, one more suitable for small illumination/collection separations and one more suitable for larger ones.
- Concise analytical expressions for the description of reflectance sampling depth for various specific geometrical configurations can be developed based on the two previous simple expressions.
- Average illumination/collection separation is confirmed to be the single most important parameter in modeling sampling depth of various reflectance geometrical configurations.

References

1. S. L. Jacques, "Optical properties of biological tissues: a review," *Phys. Med. Biol.* **58**, R37–R61 (2013).
2. L. H. Wang, S. L. Jacques, and L. Q. Zheng, "MCML—Monte-Carlo modeling of light transport in multilayered tissues," *Comput. Methods Programs Biomed.* **47**, 131–146 (1995).
3. E. Alerstam, T. Svensson, and S. Andersson-Engels, "Parallel computing with graphics processing units for high-speed Monte Carlo simulation of photon migration," *J. Biomed. Opt.* **13**(6), 060504 (2008).
4. E. Alerstam et al., "Next-generation acceleration and code optimization for light transport in turbid media using GPUs," *Biomed. Opt. Express* **1**, 658–675 (2010).
5. S. C. Kanick et al., "Monte Carlo analysis of single fiber reflectance spectroscopy: photon path length and sampling depth," *Phys. Med. Biol.* **54**, 6991–7008 (2009).
6. M. Canpolat and J. R. Mourant, "Particle size analysis of turbid media with a single optical fiber in contact with the medium to deliver and detect white light," *Appl. Opt.* **40**(22), 3792–3799 (2001).
7. F. van Leeuwen et al., "In vivo quantification of the scattering properties of tissue using multi-diameter single fiber reflectance spectroscopy," *Biomed. Opt. Express* **4**(5), 696–708 (2013).
8. G. Zonios et al., "Diffuse reflectance spectroscopy of human adenomatous colon polyps in vivo," *Appl. Opt.* **38**, 6628–6637 (1999).
9. G. Mantis and G. Zonios, "Simple two-layer reflectance model for biological tissue applications," *Appl. Opt.* **48**, 3490–3496 (2009).
10. G. Zonios and A. Dimou, "Modeling diffuse reflectance from homogeneous semi-infinite turbid media for biological tissue applications: a Monte Carlo study," *Biomed. Opt. Express* **2**, 3285–3294 (2011).
11. G. Zonios, "Reflectance model for acetowhite epithelium," *J. Biomed. Opt.* **17**(8), 087003 (2012).
12. A. J. Gomes and V. Backman, "Algorithm for automated selection of application-specific fiber-optic reflectance probes," *J. Biomed. Opt.* **18**(2), 027012 (2013).
13. A. Amelink and H. J. Sterenborg, "Measurement of the local optical properties of turbid media by differential path-length spectroscopy," *Appl. Opt.* **43**(15), 3048–3054 (2004).

Biographies of the authors are not available.